

Area-selective atomic layer deposition of molybdenum oxide


Cite as: J. Vac. Sci. Technol. A **38**, 042406 (2020); <https://doi.org/10.1116/6.0000219>


Submitted: 28 March 2020 . Accepted: 19 May 2020 . Published Online: 17 June 2020

 Julie Nitsche Kvalvik,  Jon Borgersen,  Per-Anders Hansen, and  Ola Nilsen

COLLECTIONS

Paper published as part of the special topic on [Special Topic Collection on Area Selective Deposition](#)

 This paper was selected as Featured

 This paper was selected as Scilight



View Online



Export Citation



CrossMark

ARTICLES YOU MAY BE INTERESTED IN

[Understanding chemical and physical mechanisms in atomic layer deposition](#)

The Journal of Chemical Physics **152**, 040902 (2020); <https://doi.org/10.1063/1.5133390>

[Atomic layer deposition of metals: Precursors and film growth](#)

Applied Physics Reviews **6**, 041309 (2019); <https://doi.org/10.1063/1.5087759>

[Conformality in atomic layer deposition: Current status overview of analysis and modelling](#)

Applied Physics Reviews **6**, 021302 (2019); <https://doi.org/10.1063/1.5060967>

HIDEN
ANALYTICAL

Instruments for **Advanced Science**

- Knowledge,
- Experience,
- Expertise

[Click to view our product catalogue](#)

Contact Hiden Analytical for further details:

www.HidenAnalytical.com
info@hiden.co.uk



Gas Analysis

- ▶ dynamic measurement of reaction gas streams
- ▶ catalysis and thermal analysis
- ▶ molecular beam studies
- ▶ dissolved species probes
- ▶ fermentation, environmental and ecological studies



Surface Science

- ▶ UHVTPD
- ▶ SIMS
- ▶ end point detection in ion beam etch
- ▶ elemental imaging - surface mapping



Plasma Diagnostics

- ▶ plasma source characterization
- ▶ etch and deposition process reaction kinetic studies
- ▶ analysis of neutral and radical species



Vacuum Analysis

- ▶ partial pressure measurement and control of process gases
- ▶ reactive sputter process control
- ▶ vacuum diagnostics
- ▶ vacuum coating process monitoring

Area-selective atomic layer deposition of molybdenum oxide



Cite as: J. Vac. Sci. Technol. A 38, 042406 (2020); doi: 10.1116/6.0000219

Submitted: 28 March 2020 · Accepted: 19 May 2020 ·

Published Online: 17 June 2020



View Online



Export Citation



CrossMark

Julie Nitsche Kvalvik,¹  Jon Borgersen,²  Per-Anders Hansen,¹  and Ola Nilsen^{1,a)} 

AFFILIATIONS

¹Centre for Materials Science and Nanotechnology, Department of Chemistry, University of Oslo, Postboks 1033, Blindern, 0315 Oslo, Norway

²Centre for Materials Science and Nanotechnology, Department of Physics, University of Oslo, Postboks 1048, Blindern, 0315 Oslo, Norway

Note: This paper is a part of the Special Topic Collection on Area Selective Deposition.

Electronic mail: ola.nilsen@kjemi.uio.no

ABSTRACT

Area-selective bottom-up synthesis routes of thin films are required to overcome the current limits in lithography, and such growth can be achieved with high quality and nanometer thickness control by area-selective atomic layer deposition (AS-ALD). However, the current range of materials demonstrated deposited by AS-ALD is limited, and no processes for molybdenum oxide have been available so far. In this work, the authors explore the properties of a new ALD precursor, MoCl₄O, for deposition of molybdenum oxides by ALD. MoCl₄O is administered at room temperature during deposition, making it readily available for use. When reacted with a combination of water and ozone, it leads to an AS-ALD process for deposition of MoO_x—the first reported. The process is perfectly selective for growth on glass as compared to Si(100) substrates for deposition temperatures between 200 and 300 °C, with a growth rate of 0.72 Å/cycle at 300 °C. The process is attempted on a range of substrates proving good growth on soda-lime glass and LiF and no growth on Si(100), silica, Na₂CO₃, CaCO₃, Li₃PO₃, or Li₂SiO₃. The findings of this study indicate an *activated* process by diffusion of sodium or lithium through the film during growth. The obtained films have further been characterized by x-ray photoelectron spectroscopy, scanning electron microscopy, x-ray diffraction, and atomic force microscopy, revealing films with an RSM roughness of 23 nm with the presence of crystalline MoO₂ (C P/m) when deposited at 300 °C and crystalline Mo₉O₂₆ when deposited at 250 °C. The rough MoO_x thin films may be applicable for electrocatalysis, gas sensors, or lithium-ion batteries. The findings of this study enable AS-ALD synthesis of molybdenum oxide with excellent selectivity not dependent on intermittent etching cycles during growth.

Published under license by AVS. <https://doi.org/10.1116/6.0000219>

I. INTRODUCTION

The semiconductor industry is currently approaching the limits of resolution in lithography—leaving a technology gap that may be filled with precise bottom-up synthesis approaches.¹ One obvious choice to fill this gap is by atomic layer deposition (ALD), or more specifically, area-selective ALD (AS-ALD). ALD, in general, is known to give high quality films with supreme thickness control and conformity. AS-ALD will ease processing in comparison to conventional ALD, as fewer etching steps are required. Despite the fact that the concept has been around for 15 years,² we have not seen a true boom in AS-ALD processes until now.³ This has yet to reach MoO₃, which takes part in many applications also requiring precise manufacturing, such as catalysis,^{4–6} nanostructured gas sensors,⁷ injection

layers in inverted organic photovoltaics,⁸ antibacterial coatings,⁹ electrochromic devices,¹⁰ and batteries,¹¹ among others. For applications within electrocatalysis,¹² gas sensors,¹³ or lithium-ion batteries,¹⁴ porous or rough MoO_x films can be beneficial. A whole range of techniques has already been employed to deposit MoO₃ thin films, although without area selectivity. This includes thermal evaporation,¹⁵ RF sputtering,¹⁶ flash evaporation,¹⁷ metalorganic chemical vapor deposition,¹⁸ and ALD,¹⁹ which is the subject of this study.

The range of processes for deposition of MoO₃ by ALD is limited, particularly for deposition at higher temperatures as the majority of molybdenum precursors decompose at 180 °C or below. Deposition of MoO₃ by ALD was first reported in 2010 (Ref. 19) using Mo(CO)₆ as the Mo source together with O₃ and H₂O in the

range of 152–172 °C, after which the precursor decomposes. Si $(\text{CH}_3)_3\text{cpMo}(\text{CO})_2(\eta^3\text{-2-methylallyl})$ is in like manner reported to produce MoO_3 together with O_3 at 250–300 °C.²⁰ This process does, however, require an initial heating of the Si(100) substrate at 350 °C to prevent a nucleation delay of the following MoO_x deposition. Another recent precursor for deposition of MoO_3 is bis(ethylbenzene)Mo, which together with H_2O shows ALD growth in the range of 135–150 °C.²¹ Very recently, $\text{MoO}_2(\text{iPr}_2\text{AMD})_2$ (Ref. 22) has been demonstrated as a suitable precursor to form MoO_3 up to its decomposition temperature of 175 °C using O_3 as the oxygen source. $(\text{N}^t\text{Bu})_2(\text{NMe}_2)_2\text{Mo}$ was introduced as an alternative in 2015 and forms MoO_3 with O_3 in the temperature range of 100–300 °C²³ or 50–350 °C using plasma O_2 .²⁴ The tungsten counterpart of $(\text{N}^t\text{Bu})_2(\text{NMe}_2)_2\text{Mo}$ has also been used as an ALD precursor²⁵ to form WO_3 with H_2O as the coreactant and in combination with $\text{La}(\text{thd})_3$ to form the proton-conducting ternary oxide $\text{La}_{28-x}\text{W}_{4+x}\text{O}_{54}$. The same work also mentions using WCl_4O as a W source but was not pursued further as the WCl_4O and H_2O process seemed to stop after a few cycles and had a limited growth rate. Based on the similar chemistry of Mo and W, we wanted to explore if this would also be the case for MoCl_4O or if it would work as an ALD precursor. This is the topic of this work. With MoCl_4O , we are now able to expand the MoO_x toolbox to include the $\text{MoCl}_4\text{O} + (\text{H}_2\text{O} + \text{O}_3)$ process. However, to our surprise, this system exhibits clear signs of area-selective growth, as initial experiments revealed no film on Si(100) substrates, while glass substrates were clearly coated (Fig. 1).

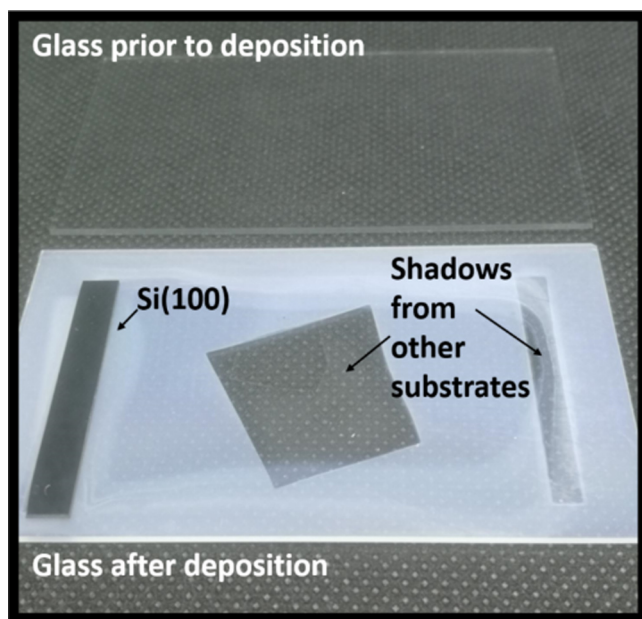


FIG. 1. Picture of an MoO_3 thin film on glass and Si deposited at 300 °C using 1000 cycles of MoCl_4O and $(\text{H}_2\text{O} + \text{O}_3)$. The film is clearly visible on the glass plate after deposition as compared to prior to deposition, but no film could be detected on the Si(100) strip.

Area-selective ALD is an emerging field particularly useful in semiconductor processing for electronics where numerous lithography steps are required.^{26,27} An overview of the field is given in Ref. 24 and can be summarized as divided into the following approaches: *Inherent* systems, where no extra measures are taken to make the system area-selective; the use of *activators*, using catalytic reactions on the surfaces, plasma enhanced areas, etc., such as for deposition of Fe_2O_3 and NiO by O_2 gas with *t*-butyl ferrocene/nickelocene on Pt and Ir substrates that dissociate O_2 , and not on the inert SiO_2 , Al_2O_3 , and Au substrates;²⁸ the use of *inhibitors*, such as for deposition of SiO_2 on GeO_2 , SiN_x , SiO_2 , and WO_3 , and not on Al_2O_3 , TiO_2 , and HfO_2 ,²⁹ where acetylacetonate chemoselectively inhibits growth by selective adsorption on the latter surfaces. Of these approaches, using inhibitors is by far the most used.

Other examples using inhibitors include the deposition of TiO_2 on gold substrates using self-assembled monolayers (SAMs) as inhibitors,³⁰ Ru on Cu lines using amino-functionalized SAMs as inhibitors,³¹ and CoO on SiO_2/MgO using polystyrene as inhibitors.³² The combination of atomic layer etching (ALE) and ALD is also employed to make thicker films only on the desired substrate. For example, Al_2O_3 has been deposited selectively on Si and not on octadecylphosphonic acid (OPDA)-SAM inhibited Cu with intermitting acid etch cycles.³³

The figure of merit for quantification of the selectivity of a system is termed selectivity, *S*, and is in Ref. 24 defined as the amount (or rate) of one product relative to the total amount (or rate) of all products formed. *S* also varies with the number of ALD cycles used and must therefore be reported together.²⁷ An example of a reported selectivity is 2000:1 for Pt versus SiO_2 substrates for the previously mentioned Fe_2O_3 system using 300 cycles.²⁸

In this study, we further explore the effect of different types of substrates on the selectivity of the $\text{MoCl}_4\text{O} + (\text{H}_2\text{O} + \text{O}_3)$ system to shed light on possible mechanisms behind our observations.

II. EXPERIMENT

A. Atomic layer deposition

All depositions were performed in an F-120 Sat reactor (ASM Microchemistry), in the temperature range of 200–350 °C. The purging gas was N_2 at $300 \text{ cm}^3 \text{ min}^{-1}$ from gas cylinders (Praxair, 99.999%, further purified through a Mykrolis purifier) providing a background pressure of ~ 4 mbar. The depositions were carried out using MoCl_4O (Sigma-Aldrich, 97%) as the Mo source and distilled H_2O and O_3 pulsed simultaneously as the O source. O_3 was supplied from an In USA ozone generator (AC-2505) at 15 wt. % O_3 in O_2 , using O_2 from a gas cylinder (Praxair, 99.5%). Both MoCl_4O and H_2O were kept at room temperature in external containers, and MoCl_4O was assisted by N_2 carrier gas. Standard pulsing times were 3 s for both MoCl_4O and $\text{O}_3 + \text{H}_2\text{O}$, followed by 3 s purging after MoCl_4O and 5 s after $\text{O}_3 + \text{H}_2\text{O}$, unless otherwise specified. The times were chosen based on experience with similar systems and gave here uniform films and reproducible data. A standard deposition consisted of 1000 cycles at a deposition temperature of 300 °C. The LiF seeding layers were deposited using LiO^tBu (Sigma-Aldrich, 97%) and NH_4F (Sigma-Aldrich, 99.99%) based on an internally developed process.³⁴ The LiO^tBu and NH_4F precursors were kept at 130 and 95 °C, respectively, and pulsed/purged with 5/5 s and 7/3 s, respectively.

A variety of substrates were used, including Si(100) with a native oxide layer, Si(100) with the following ALD-deposited thin films—CaCO₃ [from Ca(thd)₂, CO₂ and O₃ (Ref. 35)], Na₂CO₃ [from NaO^tBu, H₂O, and CO₂ (Ref. 36)], Li₃PO₃ [from LiO^tBu, Me₃PO₃, and water, and x-ray photoelectron spectroscopy (XPS) revealing a surface layer of Li₂CO₃], LiF and Li₂SiO₃ [from lithium trimethylsilanolate and H₂O (Ref. 37)]—conventional soda-lime glass containing 15 mol.% Na₂O₃ (Glaswarenfabrik Karl Heckt), and silica. Si(100), glass, and silica substrates were all washed with ethanol and blown dry prior to deposition. The other substrates were left untouched to not alter the films already deposited on them.

B. Thin film characterization

The thicknesses of the films were measured using a J. A. Woollam α -SE spectroscopic ellipsometer in the range of 390–900 nm, with the COMPLETEEASE software and Cauchy models to analyze the data. The models used two layers, one dense in the bottom and one rough on top, and took into consideration that MoO_x is absorbing. For each sample, three spots were measured. It was spot dependent how easy it was to model the ellipsometry data, probably due to variations of the roughnesses of the films. Scanning electron microscopy (SEM) was performed using a HITACHI TM3000 SEM with a working distance of \sim 9 mm and an acceleration voltage of 15 kV. A Quantax70 energy dispersive x-ray spectrometer equipped with a silicon drift detector and Cu K α radiation was used for elemental analysis. The acquisition time for each measurement was 5 min. XPS measurements were carried out using a ThetaProbe instrument from ThermoScientific. The incident x-ray beam was Al K α (1.487 keV) and 4 keV Ar⁺ was used for sputtering. The C1s peak at 285 eV stemming from carbon contamination was used as internal standard for fitting of the XPS spectra. X-ray diffraction (XRD) was performed to study the crystallinity of the samples, using a Bruker D8 Discovery Diffractometer, with Cu K α 1 radiation and a Ge(111) monochromator in a traditional Bragg–Brentano setup. Atomic force microscopy (AFM) was performed using a Park Systems XE-70 AFM equipped with a PPP-CONTSCR cantilever in the contact mode. The AFM micrographs were processed with the GWYDDION software. Four-point probe inline resistivity measurements was performed using a Keithley 2400 SourceMeter.

C. Lithography

The LiF films were patterned using photolithography. A Microposit S1813 positive photoresist was applied using a spin coater, before the sample was baked at 120 °C for 60 s on a hot plate. The pattern was exposed in a Heidelberg μ PG501 maskless lithography system and developed in the Microposit MF351 developer diluted with three parts de-ionized (DI) water. Following the development, the sample was rinsed for 1 s in DI water and immediately blown dry in N₂ gas. The exposed LiF was etched by immersing the sample in DI water for 1 min, before the photoresist was stripped by soaking in acetone for 4 min. Unfortunately, 1 min of etching time was found to be excessive, and caused a loss of resolution in the pattern, however, still suitable to prove the possible use within lithography.

D. Selectivity calculations

The selectivity is calculated using the relation given in the Introduction, namely, that selectivity is the “the amount (or rate) of one product relative to the total amount (or rate) of all products formed.”²⁷ This translates to the following equation where S is the selectivity, n is the number of cycles, and Θ_1 is the measured fraction covered by nuclei at growth surface relative to the measured fraction at an adjacent nongrowth surface, Θ_2 . The full derivation of this is found in Ref. 27,

$$S(n) = \frac{\Theta_1 - \Theta_2}{\Theta_1 + \Theta_2}. \quad (1)$$

The measured fraction covered by nuclei is directly proportional to the deposited film volume. It is therefore possible to get a measure of this by various characterization methods such as spectroscopic ellipsometry, Auger electron spectroscopy, or electron dispersive x-ray spectroscopy (EDS), which is used in this case. Here, the at. % of Mo versus (Si + Mo) is used as θ for films deposited on both glass and Si(100) substrates.

E. Thermodynamic calculations

Thermodynamic calculations were performed using the HSC CHEMISTRY 8 software from Outotec.

III. RESULTS AND DISCUSSION

A. MoO_x thin film growth

Using the standard pulsing and purging times, MoO_x was successfully deposited by atomic layer deposition with similar growth rates on glass (0.72 Å/cycle) and LiF (0.69 Å/cycle) substrates. It was possible to obtain a sufficient dose of MoCl₄O kept at room temperature when extra carrier gas was flushed through the bubbler during pulsing. The films on glass appeared light blue. Based on this, glass was used as the standard substrate for subsequent investigations. A test for chemical vapor deposition growth was performed by pulsing only MoCl₄O and keeping the reaction chamber at 300 °C. This resulted in no detectable film proving that the precursor does not decompose during operation. Initially, shorter pulsing and purging times (1s/ 1s/ 2s/ 3s) than the standard (3s/ 3s/ 3s/ 5s) mentioned in Sec. II. Experiments were tested, but this led to gradients with reduced growth along the flow direction in the reactor chamber. The standard pulsing and purging times were the shortest that also yielded even, reproducible films. No film was obtained using standard pulsing parameters on either Li₂SiO₃, Si(100) with a native oxide layer, CaCO₃, Na₂CO₃, Li₃PO₃, or silica substrates, as measured with spectroscopic ellipsometry. See the supplementary material⁵⁰ for the measured thicknesses before and after deposition.

The growth per cycle of MoO_x versus deposition temperature as grown on glass substrates is shown in Fig. 2. For 1000 cycles, the growth per cycle rapidly increases when the deposition temperature is increased from 275 to 300 °C, indicating a kinetically limited growth at temperatures below 300 °C. For 5000 cycles, there is a slight increase, although still within the error margin, between 300 and 350 °C.

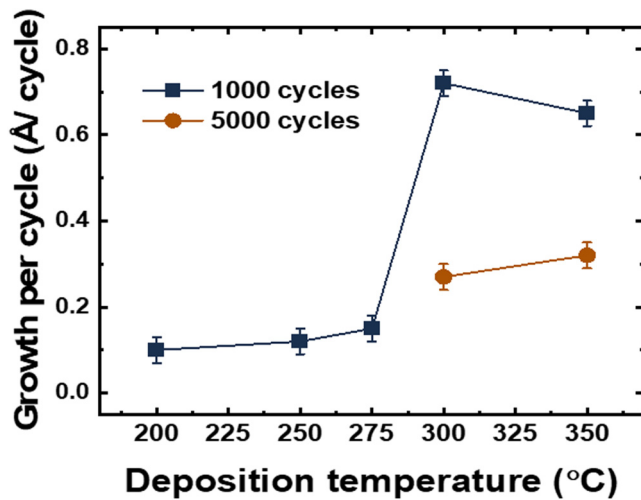


FIG. 2. Growth per cycle on glass vs deposition temperature of MoO_x for the $\text{MoCl}_4\text{O}_3/\text{O}_3 + \text{H}_2\text{O}$ system using 1000 (squares) or 5000 (circles) ALD cycles. The uncertainties are estimated from the variance in data obtained for 1000 cycles at 300 °C for three separate experiments.

The linearity with respect to the number of ALD cycles was investigated at 300 °C (Fig. 3) proving an overall reduction in growth per cycle with increased film thicknesses. ALD processes are usually regarded as linear with the number of deposition cycles, unless nucleation or evolution of texture affects the available surface area. The current observation with temperature and thickness dependent

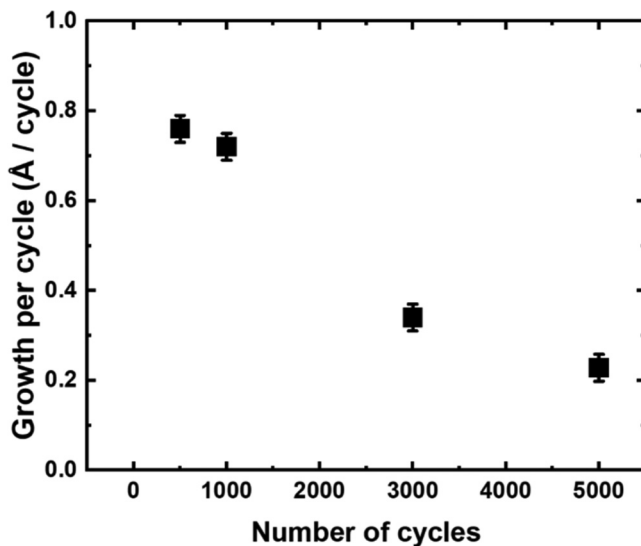


FIG. 3. Growth per cycle of MoO_x vs number of cycles for the $\text{MoCl}_4\text{O}_3/\text{O}_3 + \text{H}_2\text{O}$ at 300 °C. The uncertainties are estimated from the variance in data obtained for 1000 cycles at 300 °C for three separate experiments.

TABLE I. Growth rate of MoO_x on glass using MoOCl_4 and a selection of oxygen sources at a substrate temperature of 300 °C and 1000 cycles, as measured with spectroscopic ellipsometry.

O source	Growth per cycle (Å)
$\text{O}_3 + \text{H}_2\text{O}$ pulsed simultaneously	0.72
Only O_3	0.12
Only H_2O	0.10

growth indicates that the process may be controlled by diffusion of an active component from the substrate itself. This also explains why the growth per cycle increases between 300 and 350 °C for 5000 cycles, as the growth of thicker films is more limited by diffusion, which is in turn enhanced at higher temperatures. See the supplementary material⁵⁰ for attempts on modeling the evolution in film thickness based on diffusion limited principles.

As this system exhibits clear selectivity with respect to the substrate material, further investigations were performed to gain more insight into its origin. A first step was investigating the oxygen source, if both O_3 and H_2O play an active part in the growth. When changing the oxygen source to only H_2O or O_3 , a clear reduction of the overall growth rates was observed (Table I). A similar dependency is previously reported for when $\text{Mo}(\text{CO})_6$ is used as an Mo source, although at a reduced magnitude.¹⁹ For the $\text{Mo}(\text{CO})_6$ process, the effects of omitting H_2O was negligible, but a reduction in growth rate of about 75% was observed when omitting O_3 .

XRD analysis of the films shows a strong dependency of the crystallinity with deposition temperature (Fig. 4). Films deposited at 250 °C match well with Mo_9O_{26} (P 2/C), while the crystallinity is reduced at 275 °C, and at 300 °C, there is only one clear peak present, and this matches well with MoO_2 (C 2/m, tugarinovite). Mo_9O_{26} is a Magnéli phase with a structure closely related to the

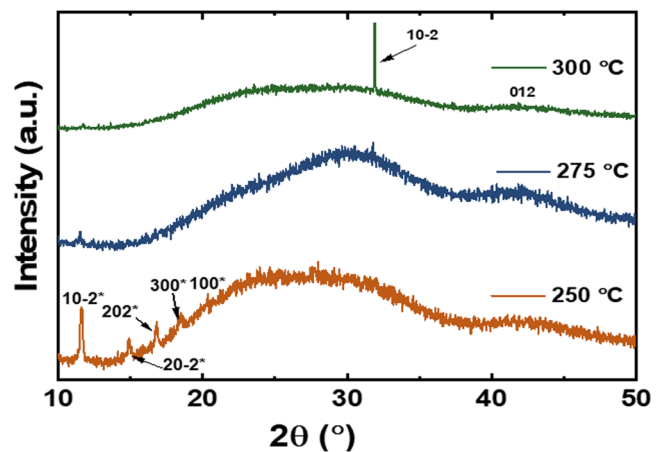


FIG. 4. XRD diffractograms of molybdenum oxide thin films deposited at varying temperatures using 1000 cycles. Selected reflexes from Mo_9O_{26} (P 2/C, with asterisk) (Ref. 42) and MoO_2 (C 2/m, tugarinovite, no asterisk) (Ref. 43) are indexed for comparison.

more common layered α - MoO_3 ,³⁸ which consists of zig-zag layers of distorted MoO_6 octahedra.³⁹ This is similar for Mo_9O_{26} , but this structure also includes crystallographic shear planes as described by Magnéli. The crystallographic shear planes reduce the overall oxidation state for Mo from +6 in α - MoO_3 to approximately +5.8 in Mo_9O_{26} without introducing oxygen vacancies. A previous study from our group, using the $\text{Mo}(\text{CO})_6 + (\text{O}_3 + \text{H}_2\text{O})$ process, showed that the films were amorphous as deposited at 167 °C, but crystallized to the metastable β - MoO_3 when annealed at 400 °C for 8 min and as α - MoO_3 when annealed at 600 °C for 8 min.⁴⁰ Another very recent study on MoO_3 from our group identifies the crystallization process as both time and temperature dependent proving crystallization of β - MoO_3 at only 185 °C when annealed for an extended amount of time (24 h).⁴¹ The formation of MoO_2 is further discussed later in the text.

The microstructure of thin films deposited on glass substrates was investigated with SEM and AFM (Fig. 5). The microstructure

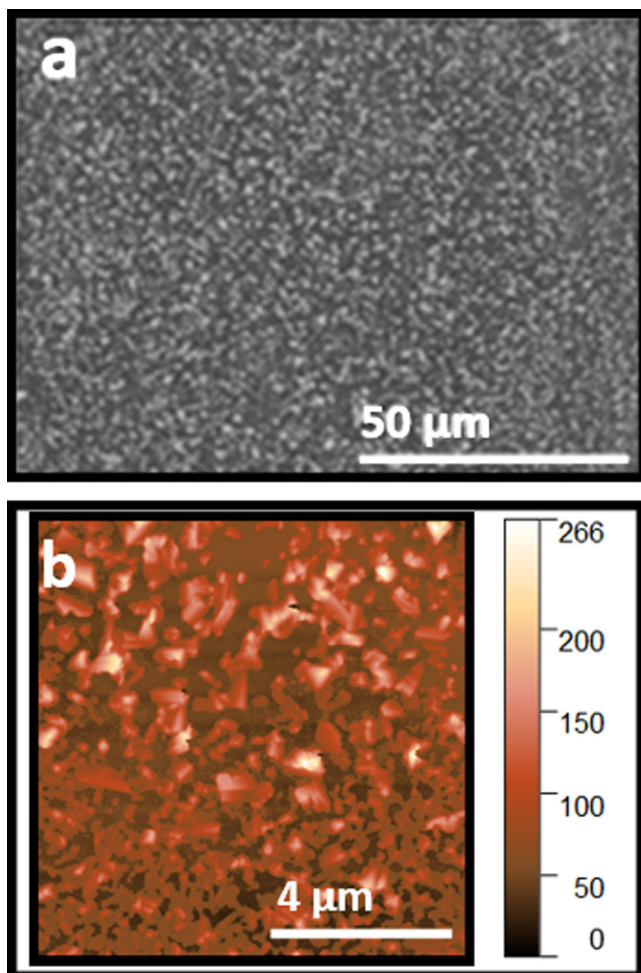


FIG. 5. SEM micrograph (a) of MoO_x deposited on glass at 250 °C and AFM micrograph (b) of MoO_x deposited on glass at 300 °C using 1000 cycles.

was similar for all investigated deposition temperatures (200–350 °C), and the micrographs in Fig. 5 are thus representative for all the investigated samples. The topography appears rough and shows some signs of pinholes. The AFM micrograph further shows that some areas are denser with a thickness around 72 nm, but some areas again have taller grains and more pinholes. The occurrence of pinholes reduces slightly with higher deposition temperatures, but the topography remains rough. The RMS roughness is 23 nm as estimated from the AFM micrograph for a film with total thickness of 72 nm. To shed more light on the film quality, a four-point probe inline resistivity measurement was performed on a 114 nm thick film deposited at 300 °C. The film was insulating at room temperature, i.e., the sheet resistance was above 100 $\text{M}\Omega/\text{sq}$.

XPS was performed on selected samples to investigate the state of molybdenum and to reveal the presence of any impurities that may be embedded in the growth process. The survey spectrum for a sample deposited at 300 °C on glass is shown in Fig. 6. This shows that beside the expected peaks from oxygen and molybdenum, a large amount of sodium is also found in the films. The Cl $p_{3/2}$ peak, which is the peak primarily used for analysis of chlorine by XPS, is normally found around 200 eV and is absent in the spectrum below.

Two XPS scans were performed on two different spots of a sample deposited at 300 °C to investigate the oxidation state of Mo (Fig. 7). For the Mo $3d_{3/2}$ peak, the peak positions are at 236.1 and 235.4 eV for the two scans, both within the expected range for the valance being +6.⁴⁴ The same goes for the Mo $3d_{5/2}$ where the peak positions are at 232.8 and 232.1 eV. The observed shift for both Mo 3d peaks between the two scans is less than expected if the valance indeed was different in the two spots.

A depth profile was also obtained by XPS on a MoO_x film deposited on glass at 300 °C, as shown in Fig. 8. It shows a relatively homogeneous distribution of sodium ions throughout the film, probably due to extended diffusion through the 2-h cooling process after the deposition. It should be kept in mind that the

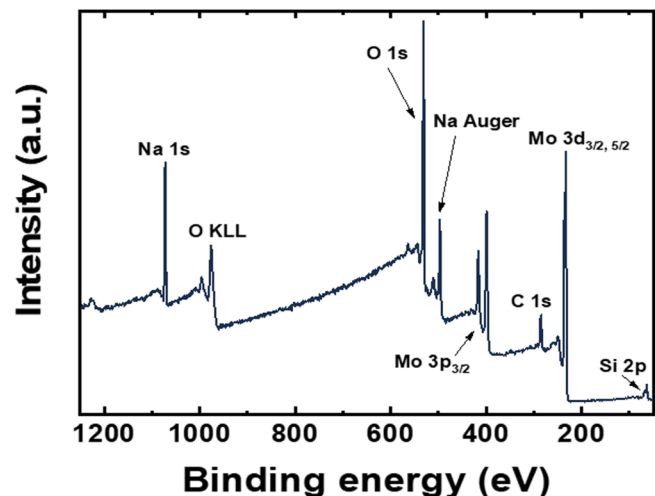


FIG. 6. XPS survey scan of MoO_x thin film deposited at 300 °C on glass.

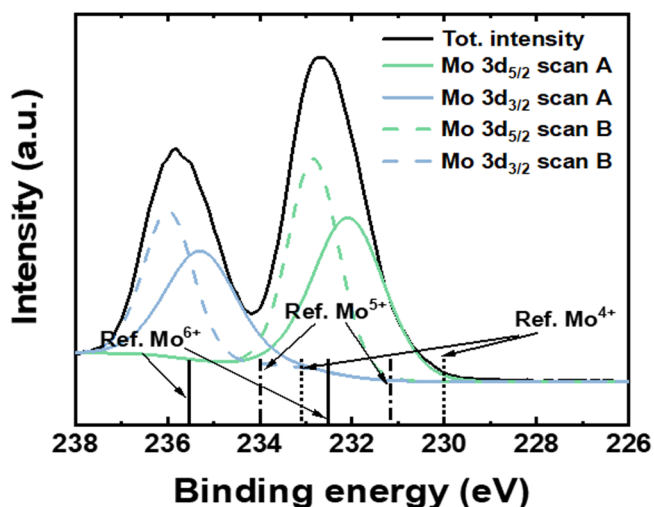


FIG. 7. XPS scans of Mo 3d peaks to identify the oxidation state of molybdenum in an MoO_x thin film deposited at 300 °C on glass. Two scans, A and B, were performed at two different spots on the same sample during the same session. Expected peak positions for Mo⁶⁺, Mo⁵⁺, and Mo⁴⁺ are included for comparison.

argon sputtering during depth profiling can also affect the distribution of sodium throughout the film. We do observe an accumulation of sodium at the surface of the film with 6.6% Na at zero etch time.

Experiments with prolonged purging times were performed to investigate how diffusion of sodium ions affect the growth rates of the MoO_x thin film. If the growth is dependent on diffusion of

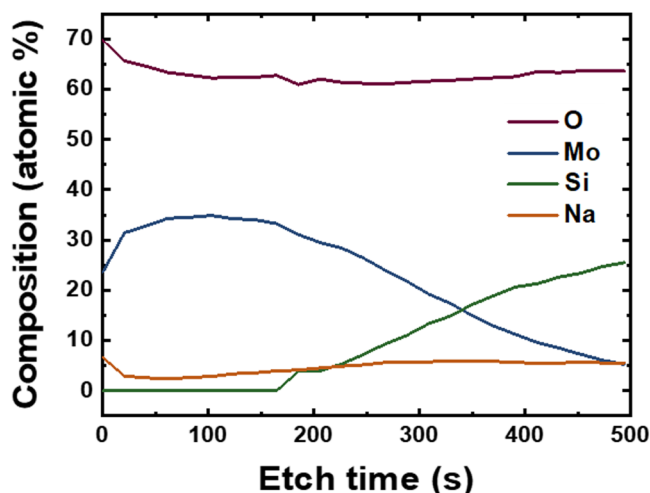


FIG. 8. XPS depth profile of MoO_x thin film as deposited at 300 °C on glass.

TABLE II. Growth rate of MoCl₄O/(O₃ + H₂O) on glass as a function of purging times at a substrate temperature of 300 °C as measured with spectroscopic ellipsometry.

Purging time after MoCl ₄ O pulse (s)	Purging time after O ₃ + H ₂ O pulse (s)	Total cycle time (s)	Growth per cycle (Å)
3	5	14	0.72
6	10	22	0.83
9	15	30	1.15

sodium through the film, the growth rate should be affected by the purging times, leading to increased growth for longer purges, as this allows for more time for diffusion controlled processes.⁴⁵ The results of such an investigation is shown in Table II and support our hypothesis, although with a higher dependency on the purging times than anticipated from Fick's laws of diffusion.

B. Area-selective growth

EDS measurements were performed on a number of samples deposited at various temperatures to quantify the selectivity of the process as a function of deposition temperature. Both growth (glass) and nongrowth [Si(100)] surfaces were investigated. As no molybdenum could be detected at the Si(100) surface for depositions at 300 °C or below, the selectivity is here reported as perfect selectivity, i.e., 1. For the film deposited at 350 °C, the selectivity was calculated from the EDS measurements to be 0.85 for glass over Si(100). See the supplementary material⁵⁰ for details about this calculation.

To illustrate the selectivity of the system further, a pattern was produced by lithography on a 45 nm thick LiF film made by ALD on Si(100). Thus, both growth and nongrowth areas were present on the same substrate. A standard MoO_x deposition was then performed on top of this patterned surface. An SEM micrograph of the resulting sample is shown in Fig. 9 where the brighter areas correspond to deposition of MoO_x. We found it challenging to perform good lithography on LiF due to its high solubility in water. Yet, samples with clear patterns were obtained.

To further illuminate the selectivity of the MoCl₄O + (H₂O + O₃) system, EDS mapping was performed on an MoO_x film deposited on patterned LiF on Si(100) (Fig. 10). Both molybdenum and fluorine are present within the desired pattern in significant amounts. Attempts to quantify the concentration of molybdenum outside this pattern result in only 0.02 at. %, whereas it revolves around 8 at. % in the pattern itself. The reported values must not be considered absolute concentrations since the EDS analysis volume penetrates through the film and into the substrate. However, they do prove a selectivity for MoO_x growth of around 400 times higher growth on the LiF pattern than in the surrounding area, even with imperfect patterning.

C. Discussion

We have here reported using the oxychloride MoCl₄O for deposition of MoO_x by atomic layer deposition. Equation (2) shows



FIG. 9. SEM micrograph (a, left) illustrating the selectivity of the MoO_x system as deposited on LiF. The pattern is the University of Oslo's logo (b, right). The LiF film under the lines of the logo shown in (b) was removed with lithography prior to deposition of MoO_x. The circle in the micrograph is the area where the EDS measurements in Fig. 10 are taken.

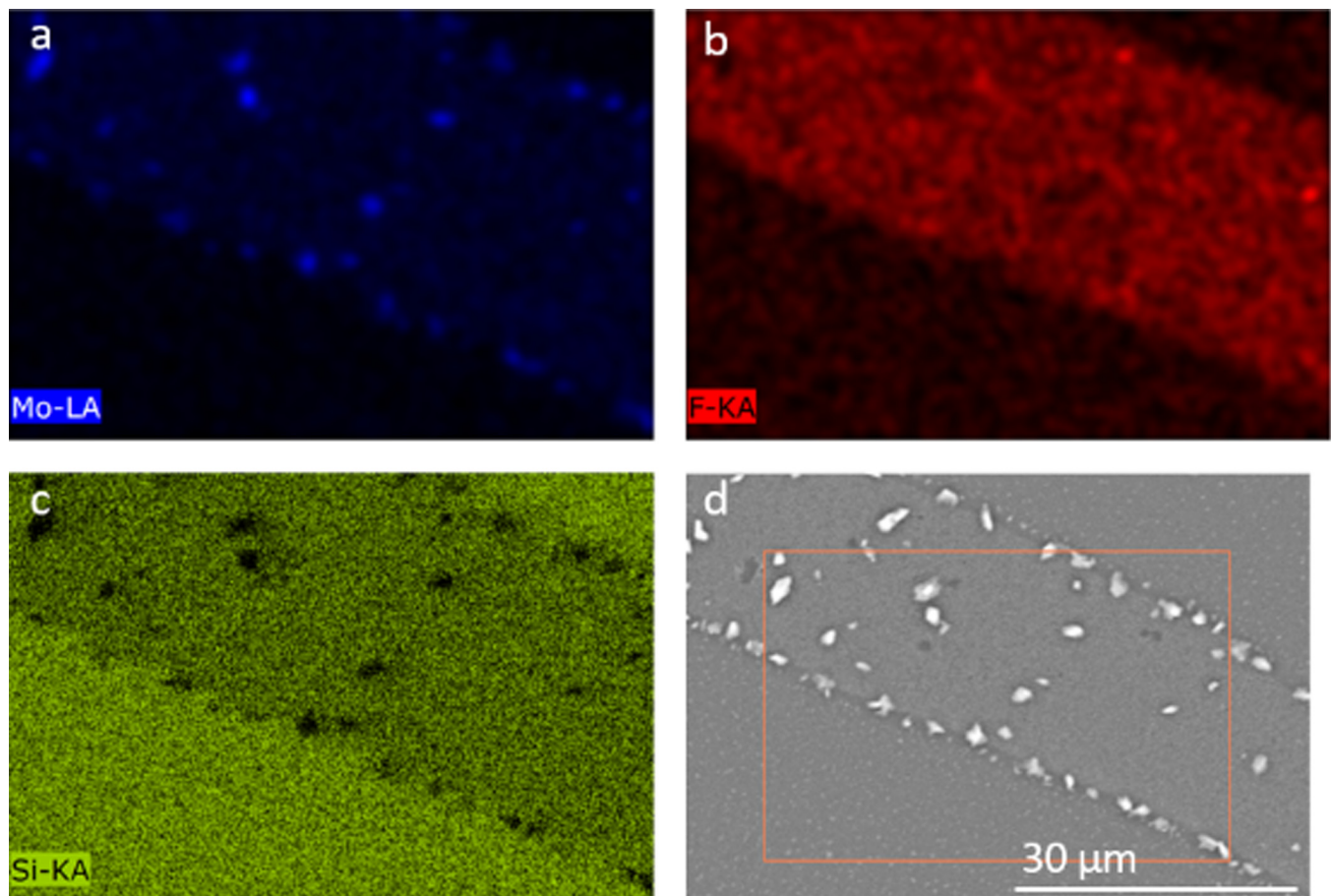


FIG. 10. EDS mapping of molybdenum L_α (a), fluorine K_α as a measure of LiF (b) and silicon K_α (c) in addition to an SEM micrograph of the surrounding area (d) of an MoO_x film deposited at 300 °C on a patterned LiF substrate. The square in subfigure (d) corresponds to the area in which the EDS measurements are performed within.

the proposed reaction between H_2O and MoCl_4O ,



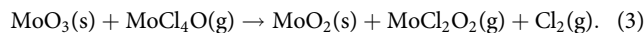
The calculated equilibrium constant, K , of this reaction is $2.3 \cdot 10^8$, $8.4 \cdot 10^7$, and $3.7 \cdot 10^7$ at 200, 250, and 300 °C, respectively. These large values point to a very favorable reaction, which is consistent with our observations. The equilibrium constant decreases one order of magnitude from 200 to 300 °C but still remain at a very high level. Even though MoCl_4O is known to thermally and photocatalytically decompose to MoCl_3O and Cl_2 already at room temperature, we still observed MoCl_4O 's distinct dark green color also after being connected to the ALD reactor in a glass bubbler with inert gas for weeks during deposition campaigns.⁴⁶

A possible reason why MoCl_4O has not previously been explored as an ALD precursor is the failed attempts to use the tungsten analog, WCl_4O , to deposit WO_3 . The previous attempts of using WCl_4O as an ALD precursor showed no growth on Si(100), but signs of growth were seen on La_2O_3 and Al_2O_3 ²⁵ when H_2O was used as the oxygen source. Likewise, we did not observe growth on Si(100), and based on our study, we would anticipate similar reaction schemes for WCl_4O as we observe for our MoCl_4O , i.e., a selective growth on alkali-containing substrates. A difference between the WCl_4O and our system is that the WO_3 films obtained on La_2O_3 and Al_2O_3 contained almost as much chlorine as tungsten. However, this may be connected with that O_3 was not used together with water in the prior study. Moreover, a very recent work studying ALE of W utilizes WCl_6 in combination with O_2 or O_3 to form volatile $\text{WCl}_4\text{O}/\text{WCl}_2\text{O}_2$ in order to etch a W surface⁴⁷ and thus the reversed chemistry. Here, thermodynamic modeling reveals that the formation of gaseous WCl_4O or WCl_2O_2 from WCl_6 and WO_3 is favorable at ≥ 200 °C.

Our study is not the first successful usage of oxychlorides as an ALD precursor. *In situ* generated NbOCl_3 has been reported to deposit Nb_2O_5 in combination with water.⁴⁸ This was revealed as the probable reason why NbCl_5 and water yielded Nb_2O_5 films with large gradients along the flow direction. NbOCl_3 was generated from NbCl_5 being pulsed into the chamber and reacting with the already present Nb_2O_5 film, thus etching the film. Based on our current findings, we expect that NbOCl_3 would work as a precursor for deposition of Nb_2O_5 also when used directly. A similar etching process as observed for NbCl_5 on Nb_2O_5 has also been seen for TaCl_5 on Ta_2O_5 but less thoroughly investigated.⁴⁹

The XRD investigations show that the type of crystalline phases depends on the deposition temperature, ranging from Mo_9O_{26} (P 2/c) at 250 °C to an XRD amorphous phase at 275 °C and MoO_2 at 300 °C. The average oxidation state of Mo in Mo_9O_{26} is 5.8+, e.g., almost 6+. XPS studies performed on a sample deposited at 300 °C shows that 6+ is the dominant valence of Mo in that sample also. This is in contrast with XRD peaks of MoO_2 for the same sample, where the oxidation state for Mo is 4+. We therefore believe the film mainly consists of an amorphous MoO_3 matrix with embedded crystalline MoO_2 islands, when deposited at 300 °C. The fact that MoO_2 is formed only at high temperatures is consistent with how the equilibrium constant, K , changes as a function

of temperature for the reaction in Eq. (3),



Here, K is $6.6 \cdot 10^{-5}$, $9.1 \cdot 10^{-4}$, and $7.9 \cdot 10^{-3}$ at 200, 250, and 300 °C, respectively, proving a two order magnitude change with temperature, suggesting why we observe MoO_2 only at high temperatures.

The growth rate of our $\text{MoCl}_4\text{O} + (\text{H}_2\text{O} + \text{O}_3)$ system showed a sudden increase from 0.13 to 0.71 Å/cycle for 1000 cycles when the deposition temperature was increased from 275 to 300 °C. Such a high thermal sensitivity of the growth rate point at a thermally activated process, such as solid-state diffusion, where exponential dependency of diffusion rate with temperature is expected.

An unusual trait of this ALD process is that the growth rate per cycle is not constant as a function of number of cycles, i.e., on the thickness of the deposited film. The growth rate slows down when the number of cycles is increased and the film becomes thicker. This means that we do not enter a typical steady-state ALD situation where the entire surface is saturated and the material deposits on itself, but rather a situation where a longer distance to the interface of the substrate limits the growth.

Studies of growth rates versus purge lengths and a nonlinear relationship between the thickness of the deposited film and number of ALD cycles suggest that the growth is limited by diffusion of Li^+/Na^+ ions through the film and that the presence of alkali ions is essential for film growth. The fact that soda-lime glass facilitates growth, but silica does not, also supports this. The XPS depth profile of film deposited on glass does show sodium throughout the entire film, proving that diffusion of sodium has taken place. Since Na_2CO_3 , Li_3PO_3 , and Li_2SiO_3 coated substrates did not induce film growth, the alkali ion cannot be in any arbitrary matrix. The Na_2CO_3 , Li_3PO_3 , and Li_2SiO_3 were all expected to be terminated by a thin carbonate layer on its surface. A possible denominator is if these carbonate layers themselves lack the feature to initiate $\text{MoCl}_4\text{O} + (\text{O}_3 + \text{H}_2\text{O})$ growth. A more thorough understanding of the growth mechanisms will be a topic for more focused studies.

Also, the SEM micrographs of our thin films deposited on glass and LiF show a grainier appearance and do not cover the surface in an optimal manner when grown on LiF. This suggests that the nucleation may be more favorable on glass than LiF, despite the near equal measured growth rate.

The selectivity of our system is near perfect for glass over Si (100) with a native oxide layer. This is to the best of our knowledge also the first report of selective area atomic layer deposition of any molybdenum containing compound. Moreover, it is indeed extreme that the selectivity retained even for as much as 1000 cycles. It is rare that a system exhibits selectivity over so many cycles, as 250 cycles is typically reported as the maximum number of cycles before extra measures, such as etching steps, are required.²⁷

Taking the extreme selectivity into account, this work has thoroughly studied the possible MoO_x growth on Si(100). As all data from EDS, SEM, and XPS point to the same conclusion, that MoO_x does not growth on Si(100) using $\text{MoCl}_4\text{O} + (\text{O}_3 + \text{H}_2\text{O})$ at temperatures of 300 °C or less, we have confidence in that the system indeed is perfectly selective within this temperature range.

IV. SUMMARY AND CONCLUSIONS

We have reported on the use of the novel precursor MoCl_4O for deposition of various molybdenum oxides with ALD using deposition temperatures between 200 and 350 °C. The highest growth rate was 0.72 Å/cycle when deposited on soda-lime glass at 300 °C. The $\text{MoCl}_4\text{O} + (\text{H}_2\text{O} + \text{O}_3)$ process is clearly dependent on the chemistry of the substrate. It shows highly area-selective growth when deposited on substrates containing available lithium or sodium, only growing on glass and LiF and not on Li_3PO_3 , CaCO_3 , Na_2CO_3 , Si(100) with a native oxide layer, or silica. Moreover, the system is perfectly selective as measured by EDS for glass over Si(100) with a native oxide layer in the temperature range of 200–300 °C. XPS analysis showed a large presence of sodium in the film deposited on glass and likewise lithium in the film deposited on LiF. This presence of mobile Li^+/Na^+ is most likely the key feature of the nucleation and growth and opens for deposition of patterned structures of molybdenum oxides.

ACKNOWLEDGMENTS

The authors would like to acknowledge the Research Council of Norway for financing this work through the TRALALALA project within the ENERGIX program (No. 244087, Julie Nitsche Kvalvik and Per-Anders Hansen) and the Norwegian Micro- and Nano-Fabrication Facility, NorFab (No. 245963, Jon Borgersen). Furthermore, the authors would like to thank Kristian B. Kvamme, Amund Ruud, and Kjetil Almaas for providing substrates and Kristian Weibye for performing the XPS measurements.

REFERENCES

- ¹B. Wu and A. Kumar, *J. Vac. Sci. Technol. B* **25**, 1743 (2007).
- ²R. Chen, H. Kim, P. C. McIntyre, D. W. Porter, and S. F. Bent, *Appl. Phys. Lett.* **86**, 191910 (2005).
- ³R. Clark, K. Tapily, K.-H. Yu, T. Hakamata, S. Consiglio, D. O'Meara, C. Wajda, J. Smith, and G. Leusink, *APL Mater.* **6**, 058203 (2018).
- ⁴L. Casagrande, L. Lietti, I. Nova, P. Forzatti, and A. Baiker, *Appl. Catal. B* **22**, 63 (1999).
- ⁵J. Sonnemans and P. Mars, *J. Catal.* **31**, 209 (1973).
- ⁶H. Chang, Q. Wu, T. Zhang, M. Li, X. Sun, J. Li, L. Duan, and J. Hao, *Environ. Sci. Technol.* **49**, 12388 (2015).
- ⁷O. M. Hussain and K. S. Rao, *Mater. Chem. Phys.* **80**, 638 (2003).
- ⁸M. S. Go, J.-M. Song, C. Kim, J. Lee, J. Kim, and M. J. Lee, *Electron. Mater. Lett.* **11**, 252 (2015).
- ⁹C. Zollfrank, K. Gutbrod, P. Wechsler, and J. P. Guggenbichler, *Mater. Sci. Eng. C* **32**, 47 (2012).
- ¹⁰Y. Liu, Y. Lv, Z. Tang, L. He, and X. Liu, *Electrochim. Acta* **189**, 184 (2016).
- ¹¹U. K. Sen and S. Mitra, *RSC Adv.* **2**, 11123 (2012).
- ¹²Y. Jin, H. Wang, J. Li, X. Yue, Y. Han, P. K. Shen, and Y. Cui, *Adv. Mater.* **28**, 3785 (2016).
- ¹³V. Guidi, G. Carlo Cardinali, L. Dori, G. Faglia, M. Ferroni, G. Martinelli, P. Nelli, and G. Sberveglieri, *Sens. Actuators B Chem.* **49**, 88 (1998).
- ¹⁴D. Zhao, J. Qin, L. Zheng, and M. Cao, *Chem. Mater.* **28**, 4180 (2016).
- ¹⁵S. K. Deb and J. A. Chopoorian, *J. Appl. Phys.* **37**, 4818 (1966).
- ¹⁶P. F. Garcia and E. M. McCarron, *Thin Solid Films* **155**, 53 (1987).
- ¹⁷C. Julien, A. Khelifa, O. M. Hussain, and G. A. Nazri, *J. Cryst. Growth* **156**, 235 (1995).
- ¹⁸R. M. Guerrero, J. R. V. Garcia, V. Santes, and E. Gomez, *J. Alloys Compd.* **434**, 701 (2007).
- ¹⁹M. Diskus, O. Nilsen, and H. Fjellvåg, *J. Mater. Chem.* **21**, 705 (2011).
- ²⁰C. E. Nanayakkara, A. Vega, G. Liu, C. L. Dezelah, R. K. Kanjolia, and Y. J. Chabal, *Chem. Mater.* **28**, 8591 (2016).
- ²¹T. L. Drake and P. C. Stair, *J. Vac. Sci. Technol. A* **34**, 051403 (2016).
- ²²T. Jurca, A. W. Peters, A. R. Mouat, O. K. Farha, J. T. Hupp, T. L. Lohr, M. Delferro, and T. J. Marks, *Dalton Trans.* **46**, 1172 (2017).
- ²³A. Bertuch, G. Sundaram, M. Saly, D. Moser, and R. Kanjolia, *J. Vac. Sci. Technol. A* **32**, 01A119 (2014).
- ²⁴M. F. J. Vos, B. Macco, N. F. W. Thissen, A. A. Bol, and W. M. M. Kessels, *J. Vac. Sci. Technol. A* **34**, 01A103 (2016).
- ²⁵K. Bergum, A. Magraso, H. Fjellvåg, and O. Nilsen, *J. Mater. Chem. A* **2**, 18463 (2014).
- ²⁶A. J. M. Mackus, A. A. Bol, and W. M. M. Kessels, *Nanoscale* **6**, 10941 (2014).
- ²⁷G. N. Parsons, *J. Vac. Sci. Technol. A* **37**, 020911 (2019).
- ²⁸J. A. Singh, N. F. W. Thissen, W.-H. Kim, H. Johnson, W. M. M. Kessels, A. A. Bol, S. F. Bent, and A. J. M. Mackus, *Chem. Mater.* **30**, 663 (2018).
- ²⁹A. Mamelì, M. J. M. Merckx, B. Karasulu, F. Roozeboom, W. M. M. Kessels, and A. J. M. Mackus, *ACS Nano* **11**, 9303 (2017).
- ³⁰E. K. Seo, J. W. Lee, H. M. Sung-Suh, and M. M. Sung, *Chem. Mater.* **16**, 1878 (2004).
- ³¹I. Zylukov, V. Madhiwala, E. Voronina, M. Snelgrove, J. Bogan, R. O'Connor, S. De Gendt, and S. Armini, *ACS Appl. Mater. Interfaces* **12**, 4678 (2020).
- ³²Z. Zhang, T. Dwyer, S. M. Sirard, and J. G. Ekerdt, *J. Vac. Sci. Technol. A* **37**, 020905 (2019).
- ³³F. S. Minaye Hashemi, C. Prasittichai, and S. F. Bent, *ACS Nano* **9**, 8710 (2015).
- ³⁴J. N. Kvalvik, K. B. Kvamme, K. Almaas, A. Ruud, H. H. Sønsteby, and O. Nilsen, "LiF by atomic layer deposition - made easy," *J. Vac. Sci. Technol. A* (submitted).
- ³⁵O. Nilsen, H. Fjellvåg, and A. Kjekshus, *Thin Solid Films* **450**, 240 (2004).
- ³⁶Ø. S. Fjellvåg, *Tynne filmer og nanobelter for batterier: Syntese og karakterisering av katodematerialer for litium- og natriumionbatterier* (University of Oslo, Oslo, Norway, 2014).
- ³⁷A. Ruud, V. Miikkulainen, K. Mizohata, H. Fjellvåg, and O. Nilsen, *J. Vac. Sci. Technol. A* **35**, 01B133 (2017).
- ³⁸A. Magneli, *Acta Cryst.* **6**, 495 (1953).
- ³⁹O. Bertrand, P. Dufour, N. Floquet, and L. C. Dufoue, *Phys. Status Solidi A* **71**, 511 (1982).
- ⁴⁰M. Diskus, O. Nilsen, H. Fjellvåg, S. Diplas, P. Beato, C. Harvey, E. Lantman, and B. Weckhuysen, *J. Vac. Sci. Technol. A* **30**, 01A107 (2012).
- ⁴¹Ø. S. Fjellvåg, A. Ruud, H. H. Sønsteby, O. Nilsen, and H. Fjellvåg, *Cryst. Growth Des.* **20**, 3861–3866 (2020).
- ⁴²H. Gruber and E. Krautz, *Phys. Status Solidi A* **62**, 615 (1980).
- ⁴³T. Leisegang, A. A. Levin, J. Walter, and D. C. Meyer, *Cryst. Res. Technol.* **40**, 95 (2005).
- ⁴⁴J. G. Choi and L. T. Thompson, *Appl. Surf. Sci.* **93**, 143 (1996).
- ⁴⁵A. Fick, *Ann. Phys.* **170**, 59 (1855).
- ⁴⁶"Tungsten and molybdenum tetrachloride oxides," in *Inorganic Syntheses* (John Wiley & Sons, Inc., New York, 1980), pp. 195–199.
- ⁴⁷W. Xie and G. N. Parsons, *J. Vac. Sci. Technol. A* **38**, 022605 (2020).
- ⁴⁸K. Knapas, A. Rahtu, and M. Ritala, *Chem. Vap. Depos.* **15**, 269 (2009).
- ⁴⁹J. Aarik, A. Aidla, K. Kukli, and T. Uustare, *J. Cryst. Growth* **144**, 116 (1994).
- ⁵⁰See supplementary material at <http://dx.doi.org/10.1116/6.0000219> for (1) measured film thicknesses before and after deposition of MoO_x at 300 °C, (2) measured at.% from EDS used for selectivity calculations and (3) modelling of thickness vs number of cycles.